Optica Applicata, Vol. XLV, No. 4, 2015
DOI: 10.5277/oa150408

Feature extraction of molten pool for laser welding quality real-time inspection

JIAN ZHANG[1, 2*], HUIJUAN YIN[1], HE HUANG[1], RUI YANG[2], JICHUN YANG[1], YINGXIN LI[1]

[1]Chinese Academy of Medical Sciences and Peking Union Medical College Institute of Biomedical Engineering, Tianjin 300192, China

[2]Tianjin University of Technology and Education, Tianjin 300222, China

[*]Corresponding author: tjuzzjj@sina.com

This paper proposed an image feature extraction method for laser welding molten pool inspection based on cellular neural network. TC4 titanium alloy thin plates were welded by Nd:YAG pulsed laser. A coaxial machine vision system was designed to acquire molten pool images. An auxiliary lighting source was employed to improve the molten pool image quality. By analyzing molten pool images, the welding defects such as fenestration or insufficient depth were identified. These results can be used as a feedback signal for laser power control. Experimental results showed that the proposed method can be used to improve laser welding quality.

Keywords: laser materials processing, process monitoring and control, image analysis.

1. Introduction

TC4 titanium alloy, with high strength and excellent corrosion resistance, is widely used for the purpose of weight reduction in aerospace or as corrosion-resistant structural material in non-aerospace industries [1]. Laser welding is the most efficient method for thin plate welding applications, due to the capability of focusing the beam power to a very small spot diameter [2].

However, thin metal plate welding is a complicated process either in conventional or newly developed methods [3]. Unsuitable welding parameters result in many defects such as unstable weld pool, substantial spatter, tendency to drop-through for large weld pools, and sag of weld pool [4]. The relationship between laser welding parameters and welding quality has been reported [5, 6]. In order to detect the welding defects and achieve quality control, proper sensing, monitoring and inspection methods are necessary. With the development of machine vision, there is a significant interest in providing real-time assessing and close-loop regulating during laser welding process [7–9].

T a b l e 1. Chemical composition of TC4.

Composition	Al	V	Fe	C	N	H	O	Ti
Content [%]	5.5–6.8	3.5–4.5	≤0.30	≤0.08	≤0.05	≤0.015	≤0.2	Rem

In this work, we present a novel method for closed-loop laser power control based on cellular neural network (CNN). A coaxial machine vision system was designed to acquire real-time images of molten pool. Molten pool edges were extracted by means of CNN algorithm with the maximum sampling speed of 20 frame/second. The thin plate fenestration or insufficient depth of fusion can be identified by analyzing molten pool images. The thin plate fenestration or insufficient depth of fusion can be acquired by analyzing molten pool images. The information of welding defects was used as a feedback signal for laser power closed-loop control. Experimental results demonstrated that this method can observably improve laser welding quality.

2. Experiment

2.1. Test-piece

TC4 thin plates, (50×50×1) mm (H×W×D), were adopted as welding test specimens. The chemical compositions of TC4 are listed in Table 1.

2.2. Experimental setup

As shown in Fig. 1, Nd:YAG laser welding emissions can be divided into three wavelength ranges associated with reflected laser light (R), thermal radiation from the weld zone (T), and higher temperature radiation from the plasma or gas cloud above the weld (P) [8].

Figure 2 shows the experimental setup. The laser welding system consists of a 300 W pulsed Nd:YAG laser with a welding head and a numerical control worktable. The Nd:YAG laser was pumped by a pulsed lamp. To obtain molten pool images without being disturbed by plasma radiation, a machine vision with coaxial auxiliary illu-

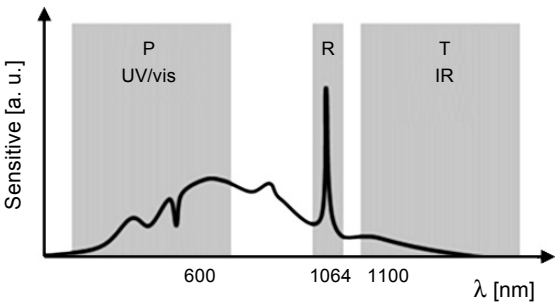

Fig. 1. A schematic of wavebands of plasma (P), reflected laser light (R), and thermal radiation (T).

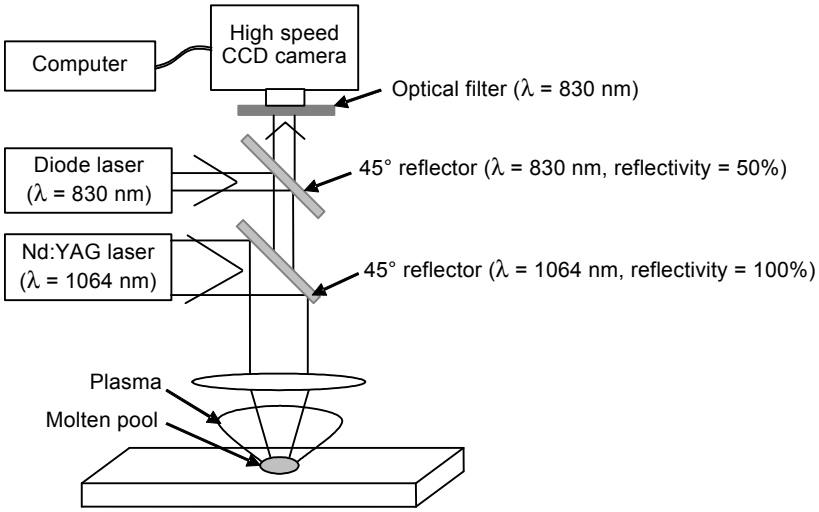

Fig. 2. Experimental setup.

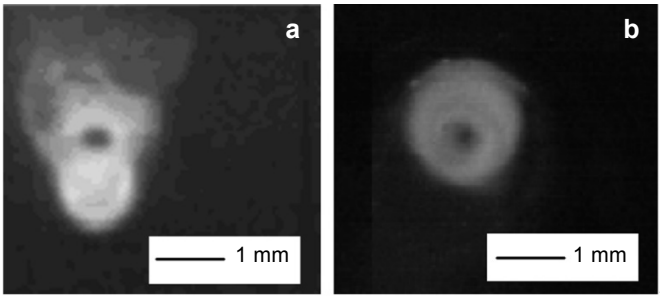

Fig. 3. Contrast of molten pool images with (**a**) and without (**b**) auxiliary illuminant.

minant system was designed. The 830 nm diode laser, with strong penetrability for plasma [8], was used as an auxiliary illuminant. Considering 10–20 ms exposure time of CCD camera, and the maximum sampling speed of 20 frame/second, the feature extraction of molten pool and closed-loop control algorithm should be accomplished within 20 ms. As shown in Fig. 3, the molten pool image quality was significantly improved with the help of an auxiliary illuminant.

2.3. Feature extraction of molten pool

CNN is a massive parallel computing paradigm defined in n-dimensional regular array of elements (cells) [10, 11]. The CNN model is a class of differential equation that has been known to have many application areas (such as noise removal, feature extraction and Chinese character recognition) and high operational speed [12]. For all time $t > 0$,

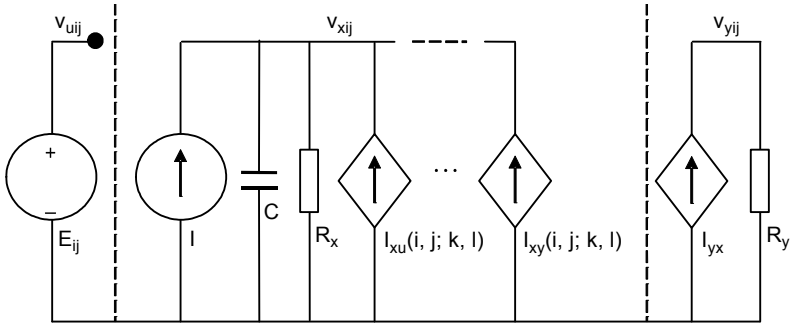

Fig. 4. Equivalent circuit of cell $c(i, j)$ – see text for explanation.

the state of each cell is said to be bounded and after the transient has settled down, a CNN always approaches one of its stable equilibrium points [13]. It implies that the circuit will not oscillate and the feature extraction of molten pool algorithm will be finished in a certain period, which is very important for laser power closed-loop control. Consider an $M\times N$ CNN, having $M\times N$ cells arranged in M rows and N columns. A typical cell $c(i, j)$ is shown in Fig. 4, where u, x and y denote the input, state and output. C is a liner capacitor; R_x and R_y are liner resistors; I is an independent voltage source, $I_{xu}(i, j; k, l)$ and $I_{xy}(i, j; k, l)$ are liner voltage-controlled current sources with the characteristics $I_{xy}(i, j; k, l) = A(i, j; k, l)v_{ykl}$ and $I_{xu}(i, j; k, l) = B(i, j; k, l)v_{ukl}$ for all $c(i, j) \in N(i, j)$; $I_{yx} = (|v_{xij} + 1| - |v_{xij} - 1|)/(2R_y)$ is a piecewise-liner voltage-controlled current source; E_{ij} is an independent voltage source [10].

Applying Kirchhoff's voltage law (KVL) and Kirchhoff's current law (KCL), the circuit equations of a cell are derived as follows:

– state equation

$$C\frac{\mathrm{d}\,v_{xij}}{\mathrm{d}t} = -\frac{1}{R_x}v_{xij}(t) + \sum_{c(k,l)\in N_r(i,j)} A(i, j; k, l)v_{ykl}(t) + \\ + \sum_{c(k,l)\in N_r(i,j)} B(i, j; k, l)v_{ukl}(t) + I, \qquad 1 \le i \le M, \quad 1 \le j \le N \tag{1}$$

– output equation

$$v_{yij}(t) = \frac{1}{2}\Big[|v_{xij}(t) + 1| - |v_{xij}(t) - 1|\Big], \qquad 1 \le i \le M, \quad 1 \le j \le N \tag{2}$$

– input equation (in practice, the magnitude of the signal can always be normalized to satisfy these conditions)

$$v_{uij} = E_{ij}, \qquad 1 \le i \le M, \quad 1 \le j \le N \tag{3}$$

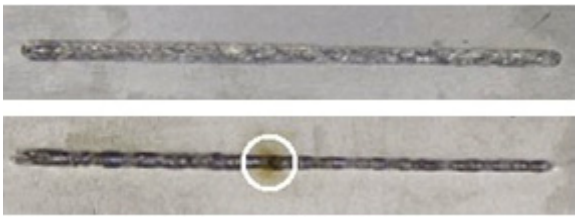

Fig. 5. Uniform welded seam with closed-loop control system (**a**). Non-uniform welded seam with open--loop control system – a welded seam perforation appears (**b**).

– constraint conditions

$$|v_{xij}(0)| \le 1, \quad 1 \le i \le M, \quad 1 \le j \le N \tag{4a}$$

$$|v_{uij}| \le 1, \quad 1 \le i \le M, \quad 1 \le j \le N \tag{4b}$$

– parameter assumptions

$$A(i,j;k,l) = A(k,l;i,j), \quad i \ge 1, \quad k \le M, \quad j \ge 1, \quad l \le N, \quad C > 0, \quad R_x > 0 \tag{5}$$

Several theorems have been proved to guarantee that the circuit, shown in Fig. 5, will not oscillate or become chaotic and the CNN has binary-value outputs [10, 11].

The common examples of edge detection algorithms are: Sobel, Canny, Laplace, Robert Cross, Prewitt, and SUSAN edge detectors. The CNN-based edge detector performed better than popular operators in terms of the computational time required, usability, and false alarm rate [14]. In this work, we used a 3×3 CNN. The circuit element parameters of the cell $c(i,j)$ were chosen as follows [11]:

$C = 10^{-9}$ F,
$R_x = 10^3$ Ω,
$I = -1.75\times10^{-3}$ A,
$A(i,j;i-1,j-1) = A(i,j;i-1,j) = A(i,j;i-1,j+1) = 0$,
$A(i,j;i,j) = 2\times10^{-3}$ Ω,
$A(i,j;i,j-1) = A(i,j;i,j+1) = 10^{-3}$ Ω,
$A(i,j;i+1,j-1) = A(i,j;i+1,j) = A(i,j;i+1,j+1) = 0$.

Figure 6 shows edge detection algorithm based on CNN.

2.4. Closed-loop control

There are two types of heating "modes" used to describe the resulting melting of the metal during laser welding, called "conduction mode" and "keyhole mode". These modes of heating are created by different power densities and produce different results. In "conduction mode" welding, the power density is great enough to cause the metal to melt. Weld penetration is achieved by the heat of the laser conducting down into

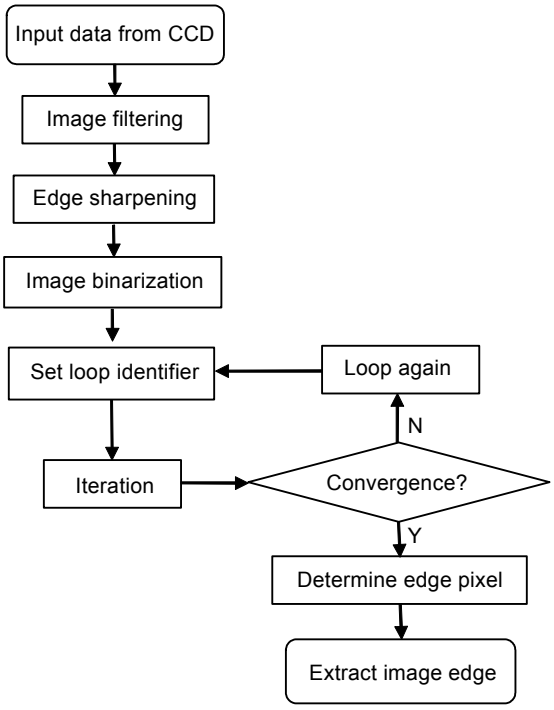

Fig. 6. Flow chart of edge detection.

the metal from the surface. Heat conduction welding is used to join thin-wall parts [15]. However, too high or too low laser power can result in fenestration or insufficient depth of fusion during thin plates welding, Figs. 7**b**–7**d**.

In order to improve thin plates laser welding quality, we designed a closed-loop laser power control system. Figure 8 sketches the important elements from the control system of view. These are laser system, weld process, molten pool images, molten pool features, and feedback signals for the laser.

A robust and fast feedback strategy is required. A simple strategy is to start with an initial $P(0)$ and to adapt this value after every acquired molten pool image feature. If "super-narrow welded seam" is observed, a value ΔP is added to the current $P(t)$; otherwise, a value ΔP is subtracted. Thus the laser welding system reaches its operating point.

Figure 7 shows four molten pool images, 256×256 pixels, under different laser welding parameters. In conduction mode laser welding, the width of the molten pool is always typically bigger than the depth [2]. The molten pool width acquired by the machine vision system can be used to identify its depth [14]. If the heat is not able to dissipate quickly enough, the processing temperature rises above the vaporization temperature, and welded seam perforation will happen (Fig. 7**b**–7**d**). In this work, we made

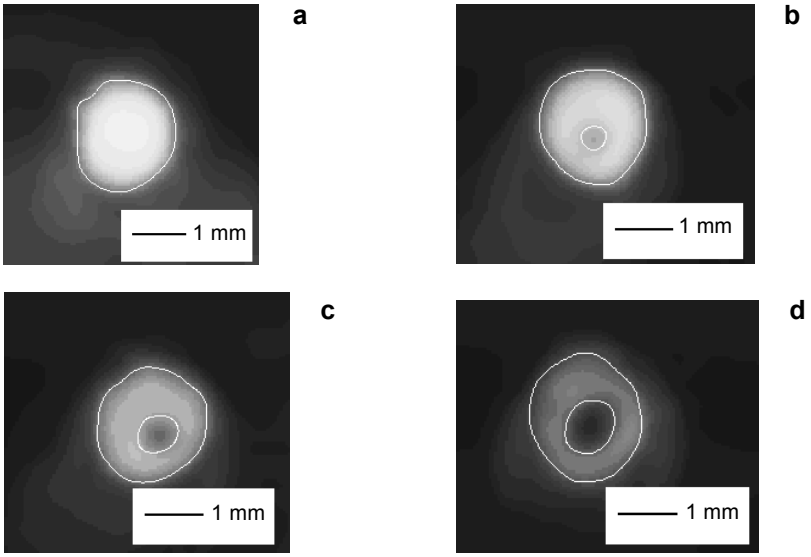

Fig. 7. Edge extraction of molten pool (see text for explanation).

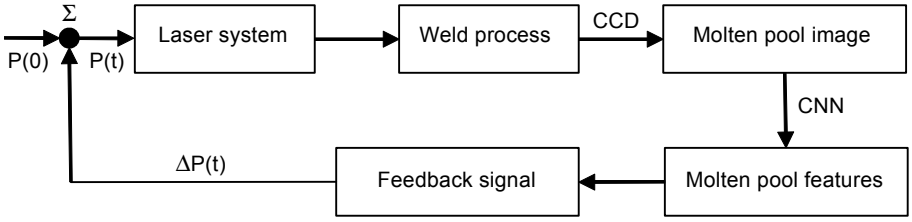

Fig. 8. Closed-loop control system.

use of the molten pool feature extraction for real-time welding quality monitoring and laser power closed-loop control. Two features were extracted from molten pool images: closed-path number N, and inner closed-path pixels number M:

1) $N \geq 1$: welded seam perforation; reduce laser power and give an alarm;
2) $N = 1$ and $M < M_{max}$: super-wide welded seam; reduce laser power;
3) $N = 1$ and $M > M_{min}$: super-narrow welded seam; raise laser power.

Parameters M_{max} and M_{min} are different values for different desired welded seam width.

3. Results

3.1. Comparison of open- and closed-loop control

Figure 9 shows the laser power fluctuation during the initial two seconds of Fig. 5**a**, laser pulse frequency is 10 Hz.

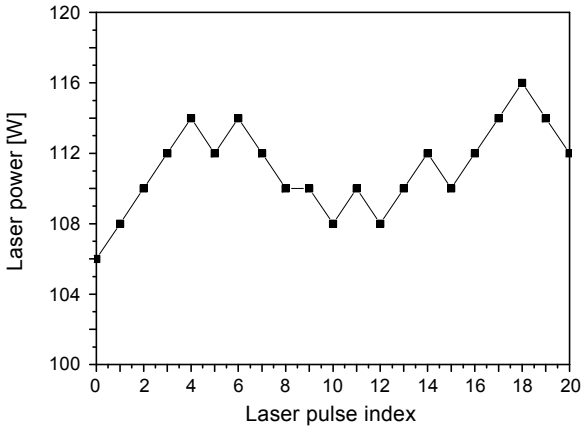

Fig. 9. Laser power fluctuation.

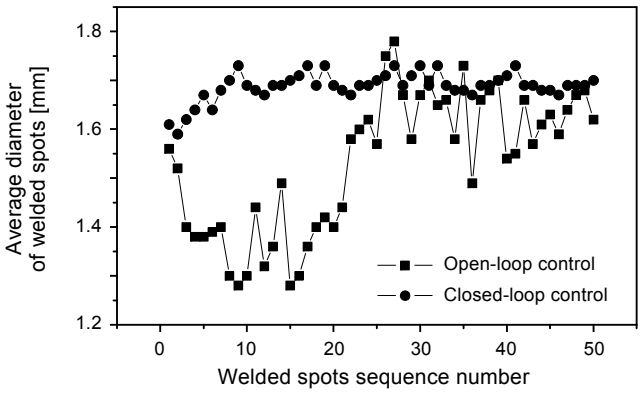

Fig. 10. Average diameter of welded spots under open- or closed-loop control.

The experiment was repeated for 50 times on open- or closed-loop conditions. Figure 10 shows an average diameter of welded spots. As can be seen, weld spot diameters are more uniform under laser power closed-loop control system.

3.2. Closed-loop control for different welded seam width

In order to verify the validity of this closed-loop control system, we repeated the laser welding experiments for different desired welded seam widths. Parameters settings and laser power fluctuations are shown in Table 2. Molten pool images are shown in Fig. 11.

3.3. The full view of molten pool

In order to observe the full view of molten pool, we conducted the experiment with (50×50×2.5) mm (W×H×D) TC4 thin plate. Figure 12 shows the surface and cross-section of molten pools.

T a b l e 2. Parameter settings and laser power fluctuations.

No.	Welded seam width [mm]	M_{max}	M_{min}	Average laser power [W]	Maximum relative deviation of laser power [%]
1	1.0	3000	3450	50	5.1
2	1.2	4500	5200	70	4.3
3	1.5	7000	8050	110	6.0
4	1.8	10100	11600	160	7.5
5	2.0	12500	14400	190	6.3

Fig. 11. Molten pool images (see Table 2).

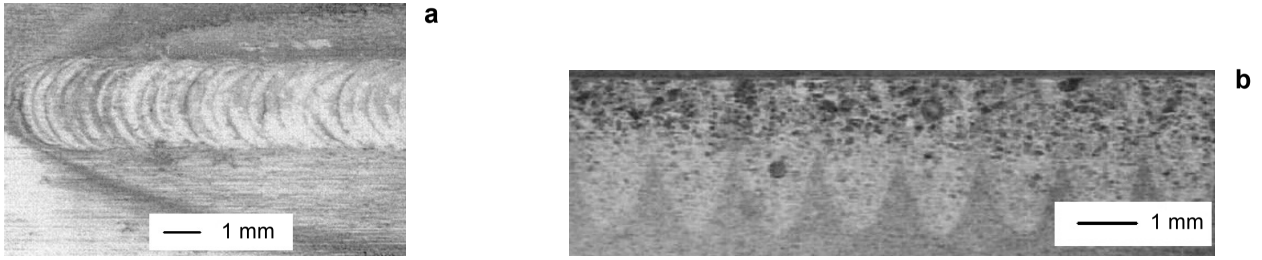

Fig. 12. Full view of molten pool. Welded seam surface (**a**), and cross-section of welded seam (**b**).

4. Conclusions

In this work, we proposed a closed-loop laser power control method. A coaxial machine vision system was designed to acquire molten pool images. A coaxial auxiliary illuminant was adopted to improve the image quality of molten pool. The molten pool features were extracted by means of CNN algorithm. By analyzing molten pool images, the welding defects such as fenestration or insufficient depth could be identified. The results from these images can be used as a feedback signal for laser power control. Experimental results demonstrated that the proposed method can efficiently improve laser welding quality.

Acknowledgments – This work was supposed by the National Natural Science Foundation of China (No. 81201819).

References

[1] HONGGANG DONG, ZHONGLIN YANG, ZENGRUI WANG, DEWEI DENG, CHUANG DONG, *Vacuum brazing TC_4 titanium alloy to 304 stainless steel with Cu-Ti-Ni-Zr-V amorphous alloy foil*, Journal of Materials Engineering and Performance **23**(10), 2014, pp. 3770–3777.

[2] ARIF A.F.M., AL-OMARI A.S., YILBAS B.S., AL-NASSAR Y.N., *Thermal stress analysis of spiral laser -welded tube*, Journal of Materials Processing Technology **211**(4), 2011, pp. 675–687.

[3] SATTARI S., BISADI H., SAJED M., *Mechanical properties and temperature distributions of thin friction stir welded sheets of AA5083*, International Journal of Mechanics and Applications **2**(1), 2012, pp. 1–6.

[4] DEMIR A., AKMAN E., CANEL T., ERTÜRK S., ARSLAN KAYA A., *Optimization of Nd:YAG laser welding of magnesium*, Journal of Laser Micro/Nanoengineering **2**(1), 2007, pp. 108–113.

[5] KABIR A.S.H., CAO X., MEDRAJ M., WANJARA P., CUDDY J., BIRUR A., *Effect of welding speed and defocusing distance on the quality of laser welded Ti-6Al-4V*, Laser Applications in Materials Processing, October 17–21, 2010, Houston, Texas, USA, pp. 2787–2797.

[6] WEI HUANG, KOVACEVIC R., *A laser-based vision system for weld quality inspection*, Sensors **11**(1), 2011, pp. 506–521.

[7] KAWAHITO Y., MIZUTANI M., KATAYAMA S., *Investigation of high-power fiber laser welding phenomena of stainless steel*, Transactions of JWRI **36**(2), 2007, pp. 11–15.

[8] OLSSON R., ERIKSSON I., POWELL J., LANGTRY A.V., KAPLAN A.F.H., *Challenges to the interpretation of the electromagnetic feedback from laser welding*, Optics and Lasers in Engineering **49**(2), 2011, pp. 188–194.

[9] TORRES-TREVIÑO L.M., REYES-VALDES F.A., LÓPEZ V., PRAGA-ALEJO R., *Multi-objective optimization of a welding process by the estimation of the Pareto optimal set*, Expert Systems with Applications **38**(7), 2011, pp. 8045–8053.

[10] CHUA L.O., YANG L., *Cellular neural networks: theory,* IEEE Transactions on Circuits and Systems **35**(10), 1988, pp. 1257–1272.

[11] CHUA L.O., YANG L., *Cellular neural networks: applications*, IEEE Transactions on Circuits and Systems **35**(10), 1988, pp. 1273–1290.

[12] NICOLOSI L., TETZLAFF R., ABT F., BLUG A., HOFLER H., *Cellular neural network (CNN) based control algorithms for omnidirectional laser welding processes: experimental results*, IEEE 12th International Workshop on Cellular Nanoscale Networks and Their Applications (CNNA), February 3–5, 2010, Berkeley, CA, pp. 1–6.

[13] PONALAGUSAMY R., SENTHILKUMAR S., *Investigation on Multilayer Raster Cellular Neural Network by Arithmetic and Heronian Mean RKAHeM(4,4)*, Proceedings of the World Congress on Engineering 2007, July 2–4, 2007, London, U.K., pp. 181–186.

[14] GAZI O.B., BELAL M., ABDEL-GALIL H., *Edge detection in satellite image using cellular neural network*, International Journal of Advanced Computer Science and Applications **5**(10), 2014, pp. 61–70.

[15] BAG S., DE A., *Development of efficient numerical heat transfer model coupled with genetic algorithm based optimisation for prediction of process variables in GTA spot welding*, Science and Technology of Welding and Joining **14**(4), 2009, pp. 333–345.

Received May 18, 2015
in revised form July 26, 2015